Evaluation of bio-optical inversion of spectral irradiance measured from an autonomous underwater vehicle

Mark A. Moline, Ian Robbins, Brian Zelenke, W. Scott Pegau, and Hemantha Wijesekera

Autonomous underwater vehicles (AUVs) can map water conditions at high spatial (horizontal and vertical) and temporal resolution, including under cloudy conditions when satellite and airborne remote sensing are not feasible. As part of the RADYO program, we deployed a passive radiometer on an AUV in the Santa Barbara Channel and off the coast of Hawaii to apply existing bio-optical algorithms for characterizing the optical constituents of coastal seawater (i.e., dissolved organic material, algal biomass, and other particles). The spectral differences between attenuation coefficients were computed from ratios of downwelling irradiance measured at depth and used to provide estimates of the in-water optical constituents. There was generally good agreement between derived values of absorption and concurrent measurements of this inherent optical property in Santa Barbara Channel. Wave focusing, cloud cover, and low attenuation coefficients influenced results off the coast of Hawaii and are used to evaluate the larger-scale application of these methods in the near surface coastal oceans.

1. Introduction

[2] Synoptic characterization of optical properties at a given location relies on above water remote sensing from satellites and airborne platforms. Dependent on location, these observations can be highly impacted by aerosols and cloud cover, are weighted to characterizing surface waters, and often do not provide continuous coverage. The predominant method of characterizing water column optical properties has been with in situ sensors on moorings either at fixed depths [*Smith et al.*, 1991; *Dickey et al.*, 1998] or with profiling capabilities [*McManus et al.*, 2003]. While providing important measurements independent of cloud cover at high temporal resolutions, these approaches lack spatial coverage. As highlighted by *Dickey et al.* [2008], the development and application of autonomous underwater vehicles (AUVs) by the oceanographic community allows for addressing both temporal and spatial scales of interest. Integration of optical sensors into AUVs allows for unprecedented resolution of the vertical and horizontal distribution of optical constituents given the flexibility in flight patterns [*Griffiths et al.*, 2001; *Griffiths*, 2002; *Moline et al.*, 2005; *Rudnick and Perry*, 2003; *Dickey et al.*, 2008] and ability for adaptive sampling of the surrounding environment [*Popa et al.*, 2004; *Leonard et al.*, 2007; *McGann et al.*, 2009]. There have been a number of recent examples using AUVs to evaluate optical variability and dynamics in the ocean. *Yu et al.* [2002] was one of the first to integrate optical backscatter in an AUV to evaluate particle resuspension events in Massachusetts Bay. Using the large Autosub AUV, *Cunningham et al.* [2003] were able to integrate a number of relatively large commercial instruments to map an optical frontal boundary and attribute changes in inherent optical properties (IOPs) to changes in phytoplankton community structure. These measurements were well correlated with satellite remote sensing and with discrete in situ samples. *Brown et al.* [2004] were the first to mount a radiometer on an AUV to quantify and map optical constituents along the coastline of New Jersey. The processes governing large scale bottom boundary dynamics and water column optical thin layers have been revealed using an AUV by *Ryan et al.* [2005] and *Ryan et al.* [2008], respectively. Using an irradiance meter integrated on an AUV, *Wijesekera et al.* [2005] found that variability in irradiance between 1 and 20 m spatial scales was attributed to the focusing effects of surface wave geometry, with the dominant wavelength of focusing at depths of 2–6 m about 2 m. With the development of a hyperspectral absorption meter [*Millie et al.*, 1997; *Kirkpatrick et al.*, 2003] and integration into an AUV, *Robbins et al.* [2006] were able to delineate and quantify the concentration of a target harmful algae species on the West Florida Shelf. *Moline et al.* [2007] used in situ reflectance measurements from radiometers integrated in an AUV to characterize and differentiate bottom habitats.

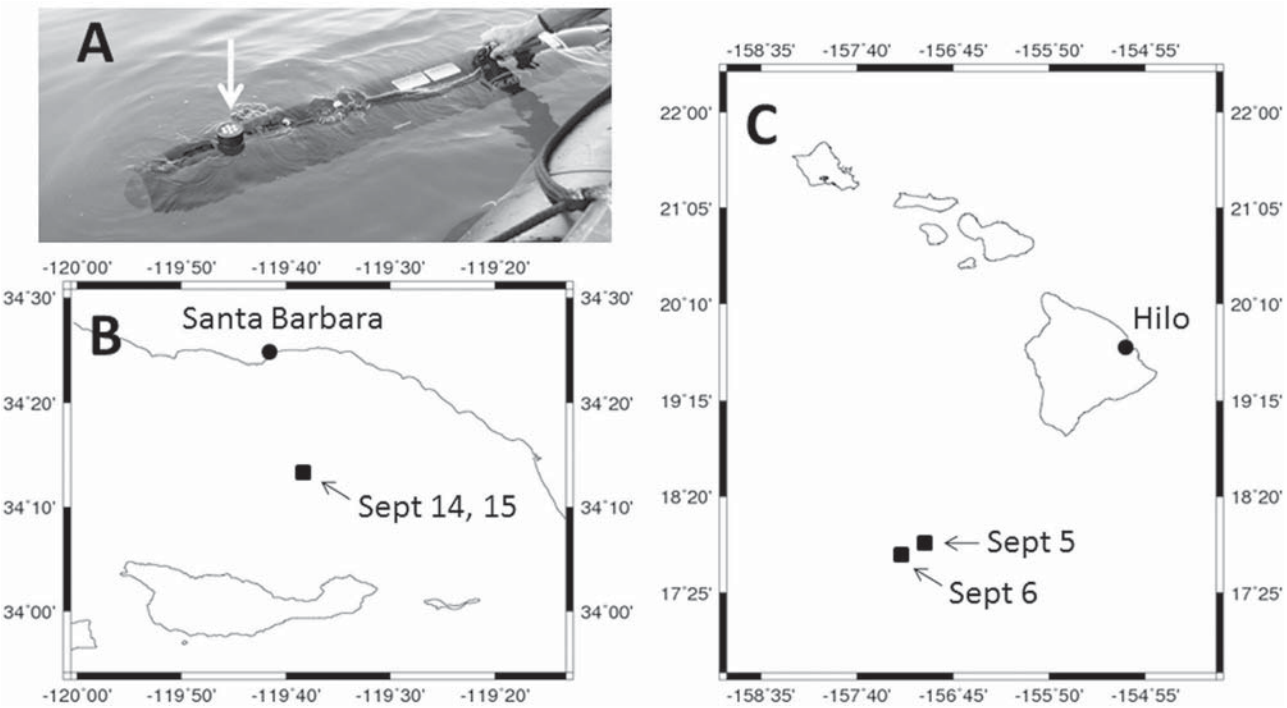

Figure 1. (a) REMUS autonomous underwater vehicle (AUV) with an integrated 7 wavelength radiometer for downwelling irradiance used in this study. Deployment sites for the AUV in (b) the Santa Barbara Channel on 14 and 15 September 2008 and (c) southwest of the island of Hawaii on 5 and 6 September 2009.

Combining a series of AUV missions in a variety of coastal environments, the sub-kilometer length scales of optical variability were quantified allowing for error prediction in the assessment of optical variability based solely on sampling resolution in these environments [*Blackwell et al.*, 2008; *Moline et al.*, 2010]. Results from these examples demonstrate the importance of integration of optical sensors in these mobile platforms to address scales of variability in the ocean not previously possible. In addition to pioneering new approaches in applying these technologies as demonstrated by these studies, it is equally important to continue to apply these approaches over a range of time and space scales in different regions to evaluate the sources of optical variability and the limits of a given technique.

[3] As part of this study, we employ a modified method developed by *Brown et al.* [2004] to quantify and evaluate the optical constituents from two field locations using an AUV outfitted with a multispectral downwelling irradiance sensor. This effort is part of the larger Radiance in a Dynamic Ocean (RaDyO) program developed to examine time-dependent oceanic radiance distribution in relation to dynamic surface boundary layer (SBL) processes, with the development of a radiance-based SBL model (T. Dickey et al., Introduction to special section, manuscript in preparation, 2012) being a primary objective. This study evaluates the highly resolved spatial/temporal variability in the optical constituents [i.e., phytoplankton, colored dissolved organic matter (cDOM), and nonalgal particulates] which directly influence the radiance distribution in the water column and can be used to inform and/or validate the SBL model. Autonomous underwater vehicles are increasing being employed in field studies in an effort to address spatial scales and variability [*Blackwell et al.*, 2008]. While they continue to demonstrate their utility in addressing scale in the ocean [*Dickey et al.*, 2008], it is important to continually assess their appropriateness for any particular application. Here, data from two optically different locations, Santa Barbara Channel and southwest of the Hawaiian Islands, were collected with an AUV to compare sites, evaluate the effects of surface conditions, and address any thresholds for universal application of this technique.

2. Methods

2.1. Field Measurements

[4] As part of the RaDyO program, a REMUS-100 AUV (Figure 1a) was deployed with a payload consisting of a Neil Brown conductivity-temperature sensor, an active fluorometer/backscatter sensor (EcoTriplet, WETLabs Inc.) measuring chlorophyll *a* (Chl *a*) fluorescence, cDOM fluorescence, and optical backscatter (650 nm), and a passive optical sensor measuring $E_d(\lambda)$ (OCR-507, Satlantic Inc.) with 7 channels centered at 412, 443, 490, 532, 555, 670, and 683 nm (HMBW = 10 nm). Data were collected at 2 Hz with a nominal vehicle speed of 1.7 m s^{-1}, yielding a horizontal data resolution of 0.85 m for the optical measurements. As mentioned by *Brown et al.* [2004], the use of spectral attenuation of downwelling light, $K_d(\lambda)$, rather than reflectance, is the basis of this analysis for a number of

reasons. In coastal regions, such as the Santa Barbara Channel, high levels of cDOM can reduce the depth at which upwelling radiance is available in the blue wavelengths to accurately estimate the amount of cDOM. *Roesler and Boss* [2003] found that in most open ocean and coastal waters attenuation is weakly influenced by backscattering and thus is not critical for inverse models of reflectance. Finally, only one sensor is required to measure the downwelling light field, eliminating the requirement for absolute synchronization between two sensors for a reflectance measurement which would be desired on a rapidly moving AUV platform.

[5] The REMUS AUV used in this study is a propeller driven platform with a length of 2 m, 19 cm in diameter, with a weight of 50 kg. Background information on the vehicle and vehicle performance is detailed by *Moline et al.* [2005]. The AUV nominally used a single dead reckoning navigation mode to complete the missions. In this mode, the vehicle used the onboard compass to maintain a bearing after submerging. As the vehicle would drift off course due to currents and known ~2.3° errors in the compass [*Moline et al.*, 2005], the vehicle was programmed to repeatedly return to the surface for a GPS fix approximately every 1–2 km (or every 10–20 min). After the GPS fix, the vehicle would attempt to reacquire the pre-programmed course. Based on the known surface GPS locations during the missions and an assumption that the drift was constant from point to point, the actual course of the vehicle was re-navigated as a post-processing step for improved location accuracy. Based on previous work, it is estimated that the difference between the reported location and the actual position was less than 50m in these open ocean conditions [*Hibler et al.*, 2008].

[6] The vehicle was deployed between 10:00 and 14:00 twice in the Santa Barbara Channel during September 2008, both under constant wind and broken cloudy sky conditions (Figure 1b). The vehicle was deployed 1 km off the coast of Santa Barbara, flew at a constant depth to the site of the RADYO experiment and conducted a series of clockwise box maneuvers beginning in the southeast corner closest to the R/V *Kilo Moana* and the R/P *Flip* (Dickey et al., manuscript in preparation, 2012). On 14 September, the vehicle conducted an undulation mission around the box (2 km per side) between 2 and 40 m, followed by a series of constant depth missions. On 15 September, the vehicle conducted the identical mission as the previous day with the addition of another undulating lap around the box. After conducting the box missions in the experimental area, the vehicle returned at constant depth to Santa Barbara for retrieval. As this study is inverting changes in irradiance as a function of depth to reveal optical constituents, only the undulation missions are used here for the inversion.

[7] The second location of deployment was ~200 km southwest of the Big Island of Hawaii (Figure 1c) (see Dickey et al., manuscript in preparation, 2012). The REMUS AUV was deployed in the morning from 09:00 to 12:00 from the R/V *Kilo Moana* in September 2009, with the vehicle on both 5 and 6 September flying "L" patterns to the southwest of the ship. On both days the vehicle undulated between 2 and 95 m on this pattern followed by constant depths before returning to the vicinity of the ship for retrieval. As the ship was drifting with consistent winds to the southwest with R/P *Flip*, there was a 20 km difference in position between the two days. There were broken clouds on both days with increased intermittency in clouds cover on the first deployment. For both locations, horizontal missions were conducted and used to evaluate effects of surface waves on the internal light field. Depths for Santa Barbara Channel were 1.5, 5, and 10 m. Depths for Hawaii were 5, 10, 15, 20, and 25 m for 5 September 2009 and 2, 4, 6, 12, 18 and 30 m on 6 September 2009. Derived data from the vehicle were also compared to the absorption coefficients measured with a WET Labs AC-S following procedures outlined by *Nencioli et al.* [2010].

2.2. Data Treatment

[8] As the calculation of $K_d(\lambda)$ is integral in deriving optical properties in the water column, a number of steps were taken to minimize the variance in $E_d(\lambda)$, including data filtering based on vehicle orientation as well as direct treatment of the $E_d(\lambda)$ data. The mean AUV pitch for this study (both field locations) was a forward incline (relative to the vehicle) of $1.2 \pm 4.3°$ (median was 1.3°). Ninety-six percent of the irradiance data were collected with attitudes less than 6°. Given the limit of 10° attitude recommended by the SeaWiFS protocols [*Mueller and Fargion*, 2002], 3% of the data set were removed. These data occurred when the vehicle would surface for occasional GPS fixes (see below) and were not part of the underway data set used in this study.

[9] Following *Brown et al.* [2004], the 670 and 683 nm wavelengths were not used in this analysis as they are influenced by sun-induced Chl *a* fluorescence [*Maritorena et al.*, 2000], Raman scattering [*Marshall and Smith*, 1990], and water absorption. Furthermore, dark values were identified for each wavelength as the value of $E_d(\lambda,z)$ when ln ($E_d(\lambda, z)$) no longer changed linearly with depth, and were then subtracted from all $E_d(\lambda,z)$ measurements. In addition, a minimum $E_d(\lambda)$ value was chosen for each wavelength as a quality control cutoff representing when the signal was too low for accurate detection. Calculations for $K_d(\lambda)$ were made over small depth intervals during both ascent and descent of the vehicle, as was done with profiling radiometers assuming that surface irradiance does not vary over the time interval between observations [*Mitchell et al.*, 2000]. The $K_d(\lambda)$ were then estimated by linear regression of the log transformed $E_d(\lambda,z)$ data over 3-m depth intervals representing 30 $E_d(\lambda,z)$ measurements (the average ascent/descent rate was ~0.2 m s^{-1} at a sampling rate of 2 Hz). The values for which the fit had a correlation coefficient lower than 0.7 were excluded from the analysis. While there may be increased error in the near surface due to wave focusing [*Wijesekera et al.*, 2005], these effects would be minimized given the vehicle was operating below 2–3 m at all times, the use of the moving averaging, and the rejection of low correlation coefficients. Following *Gordon* [1989], $K_d(\lambda)$ is a function of the absorption $a(\lambda,z)$ and backscattering coefficients $b_b(\lambda,z)$, as well as the mean cosine ($\mu_d(\lambda,z)$) with an assumed value of 0.8 independent of wavelength and optical depth. In the waters sampled, the backscattering from particles was small (less than 4% of the absorption coefficient at 488 nm) and was not included in this inversion analysis. Consistent with the inverse modeling approach of *Roesler*

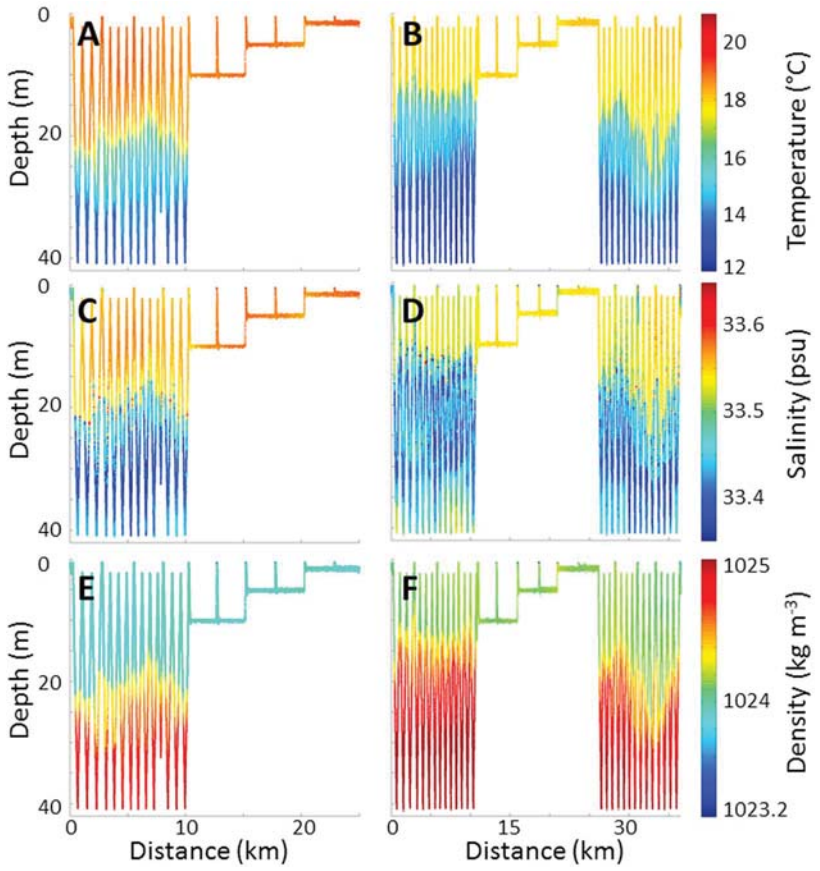

Figure 2. Depth distribution of temperature, salinity, and density as a function of distance measured by the REMUS AUV for the Santa Barbara Channel on (a, c, e) 14 September and (b, d, f) 15 September 2008. The undulating patterns were in a clockwise box pattern (Figure 1b) starting in the southeast corner. For 15 September 2008, the box was repeated.

and Perry [1995], the total absorption coefficient is represented as the sum of the absorption coefficients for the major absorbing components of seawater in the visible spectrum

$$\begin{aligned} a(\lambda,z) &= a_w(\lambda,z) + a_{ph}(\lambda,z) + a_{cm(\lambda,z)} \\ &= a_w(\lambda,z) + a_{ph}(522,z)\cdot\tilde{a}_{ph}(\lambda) + a_{cm}(412,z) \\ &\quad \cdot \exp\left[-0.0_{11\cdot(\lambda-412)}\right] \end{aligned} \tag{1}$$

where $a_w(\lambda)$, $a_{ph}(\lambda,z)$, and $a_{cm}(\lambda,z)$ are the absorption coefficients (m^{-1}) for pure seawater [*Pope and Fry*, 1997], phytoplankton, and cDOM, respectively. The parameter $a_{ph}(522,z)$ is the algal absorption coefficient (m^{-1}) at 522 nm. The term $\tilde{a}_{ph}(\lambda)$ is the spectrum for a phytoplankton absorption coefficient normalized to the average value of the spectrum over the wavelength interval 400 to 700 nm, which corresponds to the value at 522 nm (dimensionless). The spectrum used is from *Ciotti et al.* [2002] and assumes a weighting factor $S_{\langle f\rangle}$ based on the cell size distribution (0 to 1 scaling with total dominance of small cells equaling 1). In order to adapt the *Brown et al.* [2004] methods for the purposes of this experiment, the waters off Hawaii were considered dominated by picoplankton [*Takahashi and Bienfang*, 1983], $S_{\langle f\rangle} = 1$, and Santa Barbara Basin with a mixed community with $S_{\langle f\rangle} = 0.5$ [*Harding et al.*, 1982]. The cDOM component includes absorption due to cDOM and nonalgal particulates (i.e., detritus), both of which exhibit exponential decrease in absorption with wavelength. The slope of the exponential decline in the absorption coefficient for nonalgal cDOM is also adapted to local conditions and set to 0.011 nm^{-1} [*Kostadinov et al.*, 2007; *Yamashita and Tanoue*, 2009]. The inverse model uses a bounded nonlinear least squares method [*Coleman and Li*, 1994, 1996] to simultaneously fit model parameters in equation (1), representing the magnitudes of the various sources of spectral absorption. *Brown et al.* [2004] found this approach to be robust and not sensitive to the magnitude of the initial values within their normal range. The maximum bounds for all parameters were set such that they never limited the fits, and all lower bounds were set to 0. By allowing the inversion algorithm to simultaneously fit the parameters, we can obtain the individual optical contributions from various constituents, subject to the simplifications used in this analysis. To summarize the inversion algorithm, once values for K_d were obtained, the following sum was minimized

$$\sum_{\lambda}\left(K_d(\lambda,z)\cdot\bar{u}_d - \{a_w(\lambda) + a_{ph}(522,z)\cdot\bar{a}_{ph}(\lambda) + a_{cm}(412,z) \cdot \exp[-0.011\cdot(\lambda-41_2)]\}\right)^2$$

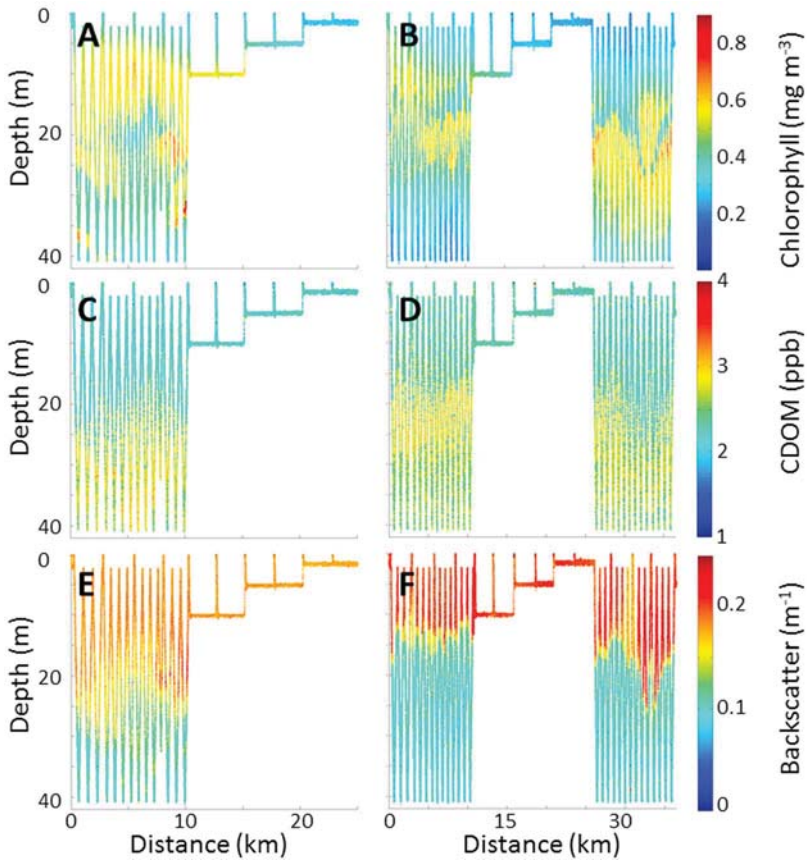

Figure 3. Depth distribution of chlorophyll *a*, CDOM and optical backscatter as a function of distance measured by the REMUS AUV for the Santa Barbara Channel on (a, c, e) 14 September and (b, d, f) 15 September 2008. Measurement patterns are identical to those in Figure 2.

by allowing $a_{ph}(522,z)$ and $a_{cm}(412,z)$ to vary and setting $\bar{u}_d$ to 0.8. An interior-reflective Newton method was used in the least squares minimization algorithm [*Coleman and Li*, 1994, 1996].

[10] Following *Wijesekera et al.* [2005], data taken from the horizontal portions of the AUV deployments in both locations were used to evaluate the effect of surface waves on the irradiance distribution in the surface waters. As the vehicle was traveling a mean speed of 1.8 m s^{-1} and the sampling rate of the irradiance sensors were 8 Hz, the effective intervals of the observations were 0.23 m. The linear distance along each depth was approximately 2 km. As the irradiance field is logarithmically dependent on depth, it was critical that the AUV maintain level flight at the predetermined depths. In this study, the shallowest depths of 1.5 m and 2 m for Santa Barbara Channel and Hawaii, respectively, presented the largest depth standard deviation of 0.1 m. Below 5 m in both sites, the standard deviation for the AUV depth at level flight was <0.06 m. Calculation of the horizontal wave number spectra were done on $E_d(490)$ for each horizontal depth specified above. The portions of each mission where the REMUS traveled at constant depths and heading, first parallel then perpendicular to the local ocean wave direction, were saved as separate time series. The 490 nm downwelling irradiance measured within each portion was selected and any missing measurements (e.g., when the REMUS paused along track to surface) were replaced with the mean of that time series. Each time series vector was then segmented into overlapping windows, of width dictated by the nearest power of two that did not exceed the length of the vector (e.g., if a time series had 1000 measured values, the nearest power of 2 is $2^9 = 512$; so the first segment would have values 1–512 and the second segment would contain values 489–1000). These segments were then passed separately into the MATLAB function psd.m, which calculated an estimate of the power spectral density and associated frequencies for each using Welch's averaged periodogram method with a Hanning window and linear de-trending [*Krauss et al.*, 1993]. The mean of the spectra and corresponding frequencies across these segments was then calculated. This power spectral density estimate for the complete time series was smoothed by band-averaging the spectra and their frequencies into 64 evenly spaced bins. Dividing the frequencies and spectra by the mean speed of the vehicle gave the wave number and spectral estimate for the irradiance time series. The MATLAB function used to derive the horizontal wave number spectra is fully commented and available

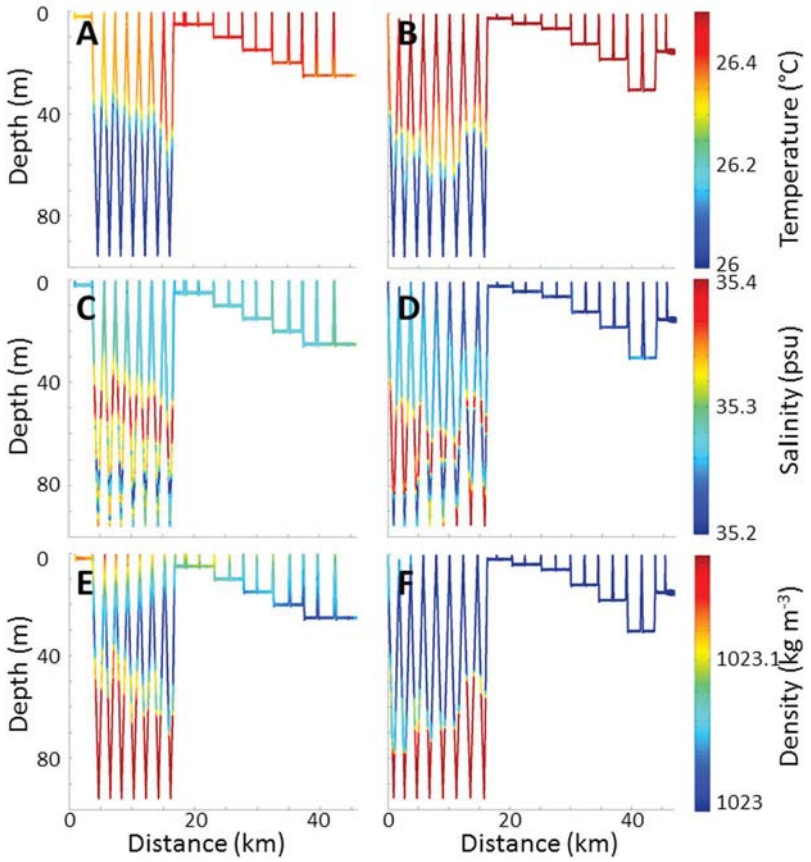

Figure 4. Depth distribution of temperature, salinity, and density as a function of distance measured by the REMUS AUV off the Hawaiian Islands (Figure 1c) on (a, c, e) 5 September and (b, d, f) 6 September 2009. The undulating patterns were in a "U" pattern starting on the northern edge.

online at (ftp://marine.calpoly.edu/Zelenke/WavenumberSpectra/TimeSeries2WavenumberPSD).

3. Results and Discussion

3.1. Environmental Variability

[11] During the AUV deployments in Santa Barbara Channel in September 2008, the water column was characterized by sharp thermoclines ranging from 10 to 20 m depth (Figure 2). The water column was 2°C warmer during 14 September than 15 September, with less variability in the depth range of the thermocline in the sampling box (Figures 2a and 2b). There was a deep excursion of the thermocline over a distance of 2 km on 15 September 2009 suggesting a possible internal wave train. Previous missions in the Santa Barbara Channel have shown extensive advection [*Otero and Siegel*, 2004], circulation [*Dong et al.*, 2009], and internal wave dynamics [*Cudaback and McPhee-Shaw*, 2009] to explain the variability in the temperature dynamics. Salinity in the upper 40 m showed similar dynamics with some indication of a deeper saline intrusion in the first undulation of 15 September 2009 (Figures 2c and 2d). Lower salinity and higher temperature resulted in a lower density in the first deployment compared to the second (Figures 2e and 2f).

[12] Chlorophyll *a* concentrations were below 1 μg L^{-1} distribution was distributed both in the mixed layer and in distinct spatial0 patches below the pycnocline both sampling days in the Santa Barbara Channel (Figures 3a and 3b). The large vertical excursion in the second deployment appears to have moved Chl *a* into the mixed layer (Figure 3b). Colored dissolved organic matter increased with depth and was in highest concentration below the pycnocline (Figures 3c and 3d). Backscatter mimicked the physical data with concentrations twice as high in the mixed layer (Figures 3e and 3f).

[13] Physical data from the Hawaii AUV deployments again showed large excursions in the thermoclines ranging from 40 to 60 m (Figures 4a and 4b). Salinity showed relatively large variation (35 to 35.5 psu) over short vertical (40 m) and horizontal scales (200 m; Figures 4c and 4d). Salinity differences were compensated by differences in temperature and resulted in a uniform density gradient with depth (Figures 4e and 4f). This density compensation has been shown in this region [*Rudnick and Ferrari*, 1999] and is the subject of ongoing work [*Shcherbina et al.*, 2010; *Smith and Ferrari*, 2009].

[14] Chlorophyll *a* and cDOM concentrations were an order of magnitude less than those measured in Santa Barbara Channel and showed a general increasing trend with depth (Figure 5). Although concentrations were low, the vertical patterns at depth were consistent with the density gradients. The general decrease in Chl *a* is likely due to low values of $K_d(\lambda)$ in these tropical waters and high

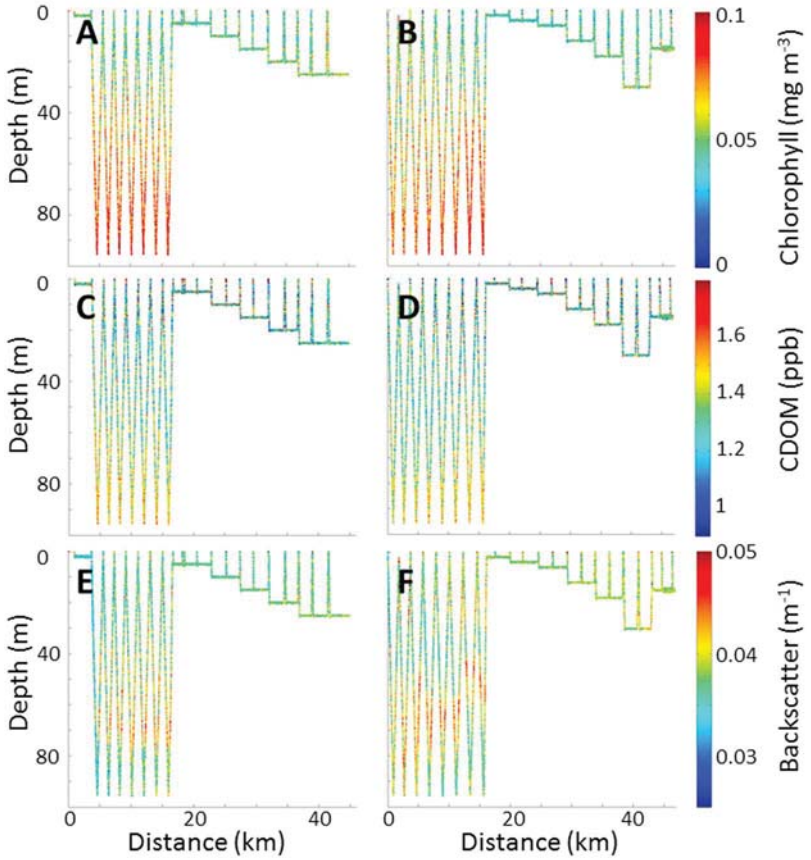

Figure 5. Depth distribution of chlorophyll *a*, CDOM and optical backscatter as a function of distance measured by the REMUS AUV off the Hawaiian Islands (Figure 1c) on (a, c, e) 5 September and (b, d, f) 6 September 2009. Measurement patterns are identical to those in Figure 4.

quenching of fluorescence, known to decrease Chl *a* concentrations by up to 80% during the midday hours [*Sackmann et al.*, 2008]. Backscatter was highest along the maximum pycnocline gradient in the upper 95 m, consistent with biogenic particles [*Nencioli et al.*, 2010].

3.2. Underwater Light Field

[15] The spectral downwelling attenuation in the Santa Barbara Channel showed high attenuation in the blue portion of the spectrum, consistent with a higher proportion of

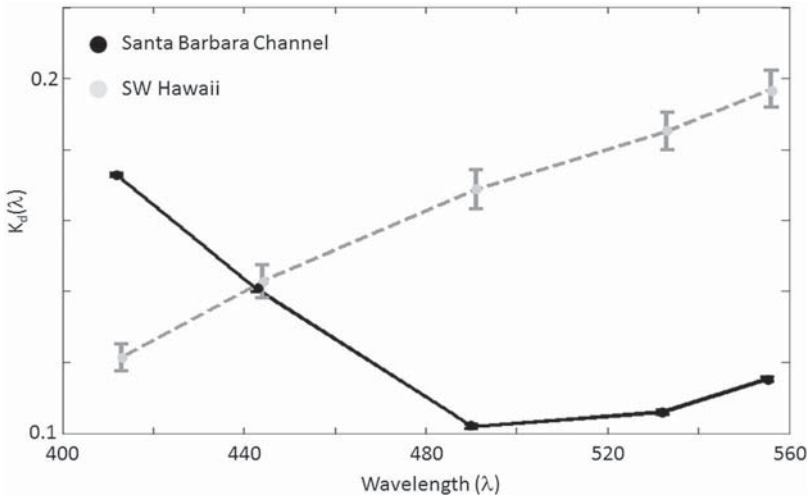

Figure 6. Mean spectral attenuation for data collected from the Santa Barbara Channel and the sampling station off the island of Hawaii. Means are shown with standard errors with wavelengths slightly offset for clarity.

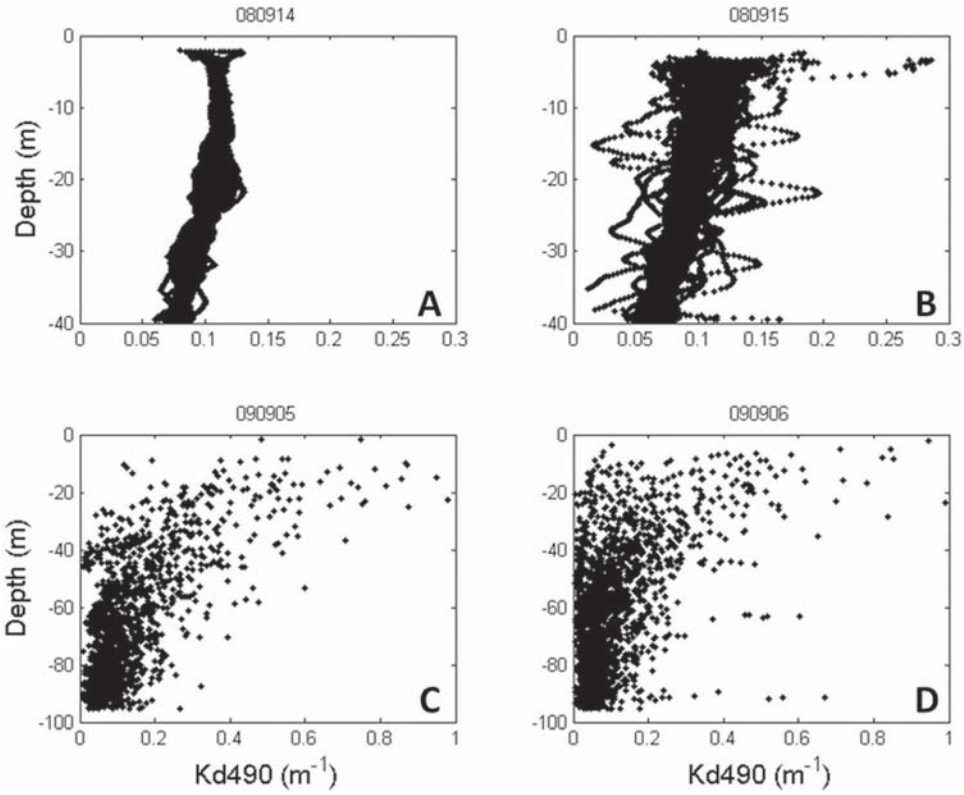

Figure 7. Downwelling attenuation coefficient at 490 nm, $K_d(490)$, as a function of depth (m) derived from AUV downwelling irradiance, $E_d(\lambda)$, measurements for Santa Barbara Channel on (a) 14 September and (b) 15 September 2008 and off the Hawaiian Islands on (c) 5 September and (d) 6 September 2009.

cDOM relative to phytoplankton (Figure 6). Even though measured attenuation by the AC-S showed values off Hawaii an order of magnitude smaller than Santa Barbara Channel (data not shown), the values of $K_d(\lambda)$ derived from the AUV deployments in Hawaii were generally higher, with a spectral shape consistent with waters with a higher proportion of phytoplankton [*Nencioli et al.*, 2010]. Even though the depth of the Chl *a* maximum was likely deeper (100 to 120 m) than the diving depth of the AUV [*Sakamoto et al.*, 2004; *Nencioli et al.*, 2010], the concentrations of Chl *a* were less than those in the Santa Barbara Channel and would not have influenced the $K_d(\lambda)$ values to the degree found in Figure 6. This inconsistency will be addressed below. Examination of the $K_d(490)$ with depth in Santa Barbara Channel shows a near uniform distribution in the surface waters to 20 m and then decreasing with depth with higher variability in the second deployment (Figures 7a and 7b). As mentioned above, $K_d(490)$ off Hawaii was higher with larger variability and showing an exponential relationship with depth (Figures 7c and 7d). This high variability suggests that surface processes were influencing this quantity. We attempted to decrease this variability by doubling the data window of the linear regression of the log transformed $E_d(\lambda,z)$ data (see section 2), but this did not significantly increase the number of points used in the analysis.

3.3. Derived Inherent Optical Properties

[16] From the inversion of $K_d(\lambda)$, we were able to derive estimates of $a_{ph}(\lambda)$ and $a_{cm}(\lambda)$. For deployments in Santa Barbara Channel, there was apparent vertical structure in $a_{ph}(490)$, with a slight increase from the surface to 15 m with a mean of 0.07 m^{-1} (Figure 8). Below this depth, there was a near linear decrease with depth of 0.001 m^{-1} m^{-1}. Measured $a_{ph}(490)$ from the AC-S cast taken within 3 h of the first deployment showed both good quantitative and qualitative agreement with both AUV deployments with peak absorption about 0.09 m^{-1} (Figure 8). The derived $a_{cm}(\lambda)$ for both the Santa Barbara Channel showed little to no vertical structure, with a mean of 0.005 m^{-1}. As the variance in the retrieved values for $K_d(\lambda)$ in Hawaii was larger than Santa Barbara Channel and also showed no vertical structure, inversion of $K_d(\lambda)$ yielded no reasonable derived values of $a_{ph}(\lambda)$ or $a_{cm}(\lambda)$. To further evaluate whether the high variability in the $K_d(\lambda)$ profiles resulted from the AUV itself (i.e., speed, dive angle), we examined profiles made from a free-falling optical cage deployed from a small boat away from the R/V *Kilo Moana*. These profiles revealed similar variance in $K_d(\lambda)$ throughout the water column increasing toward the surface (data not shown), indicating this phenomena was platform independent and resulted from the surface $E_d(\lambda)$ and wave conditions.

[17] Derived estimates of $a_{ph}(490)$ from the Santa Barbara Channel were further compared to the on board measurements of Chl *a* as seen in Figure 3 (Figure 9). The relationships show a linear agreement between the two quantities as seen in the $K_d(490)$ (Figure 8) there was less variability in the first deployment (Figure 9a). Given the known influence of fluorescence quenching with depth, the

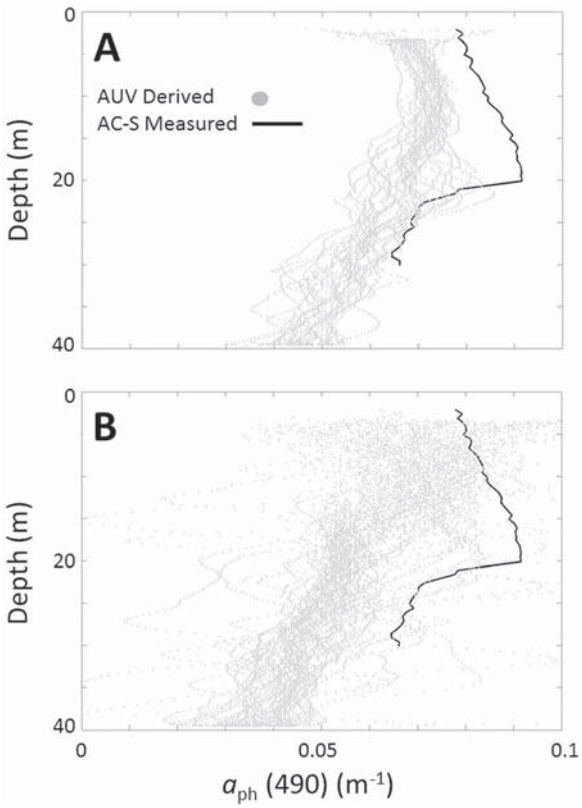

Figure 8. Derived phytoplankton absorption, a_{ph}, at 490 nm as a function of depth for Santa Barbara Channel on (a) 14 September and (b) 15 September 2008. Overlaid (black line) is the attenuation measured by the shipboard AC-S on 14 September 2008.

values were color coded to reveal the decrease in the measured Chl *a* florescence. Additionally, there was an increase in the derived $a_{ph}(490)$ at the surface. This again suggests the influence of surface $E_d(\lambda)$ and wave conditions on $K_d(\lambda)$ and the subsequent inversion approach.

3.4. Surface Waves and Internal Light Field

[18] Data from the AUV deployments from both locations showed the influence of surface conditions on deriving IOPs. In order to better evaluate this influence, the variance of $E_d(490)$ from the level flight portions of the four AUV missions (see Figures 2 and 4). There was a significant difference in the variance of $E_d(490)$ between locations and with depth (Figure 10). Highest variance was at the surface in both locations with a depth dependent order of magnitudes higher variance off Hawaii. This is consistent with high frequency changes in $E_d(\lambda)$ due to clouds, increased wave focusing effects at the surface from the wavefield [*Zaneveld et al.*, 2001; *Darecki et al.*, 2011], and lower attenuation and larger influence of these effects in Hawaii. This measure also captured the increased variance between deployments in Santa Barbara Channel and the resulting influence on the inversion estimates (Figure 10). Data from J. C. Zappa et al. (An overview of sea state conditions and air-sea fluxes during RaDyO, submitted to *Journal of Geophysical Research*, 2011) showed wave heights in Santa Barbara Channel during the deployments were 1 m with wind speeds of 5 m s^{-1}. Data off Hawaii for the AUV deployments showed both the wave heights and wind speeds were double that of Santa Barbara Channel, explaining some of the increased variance in $E_d(490)$ between locations. The variance difference between deployments in the Santa Barbara Channel could be a result of more cloud cover and diffuse light source during the first deployment relative to the second (Zappa et al., submitted manuscript, 2011).

[19] Further analysis of the influence of surface $E_d(\lambda)$ and wave focusing was conducted by evaluating the horizontal wave number spectrum of $E_d(490)$ for all four AUV deployments following *Wijesekera et al.* [2005]. Figure 11 shows horizontal wave number spectra for the data collected at level flight depths. For the Santa Barbara Channel deployments, the shape of the spectra and the offset with depth suggest there was focusing of solar rays by surface wave geometry at all scales measured. As was done by *Wijesekera et al.* [2005], we examined the possibility that the motion of the vehicle was responsible for these differences in $E_d(490)$, but found negligible impacts. For the Hawaii deployments, the spectrum is nearly constant in amplitude with depth for wave numbers <0.2 cpm (Figures 11c and 11d). The spectrum showed the smallest

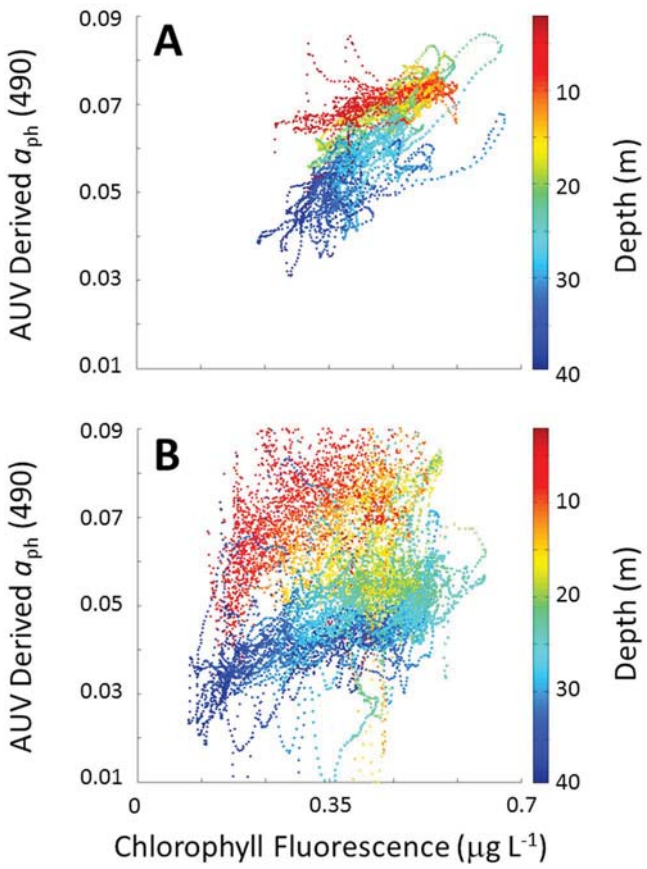

Figure 9. Relationship between derived phytoplankton absorption, a_{ph}, at 490 nm and measured chlorophyll *a* fluorescence (μg L^{-1}) for Santa Barbara Channel on (a) 14 September and (b) 15 September 2008. Overlaid color represents the depths at which the measurements were made.

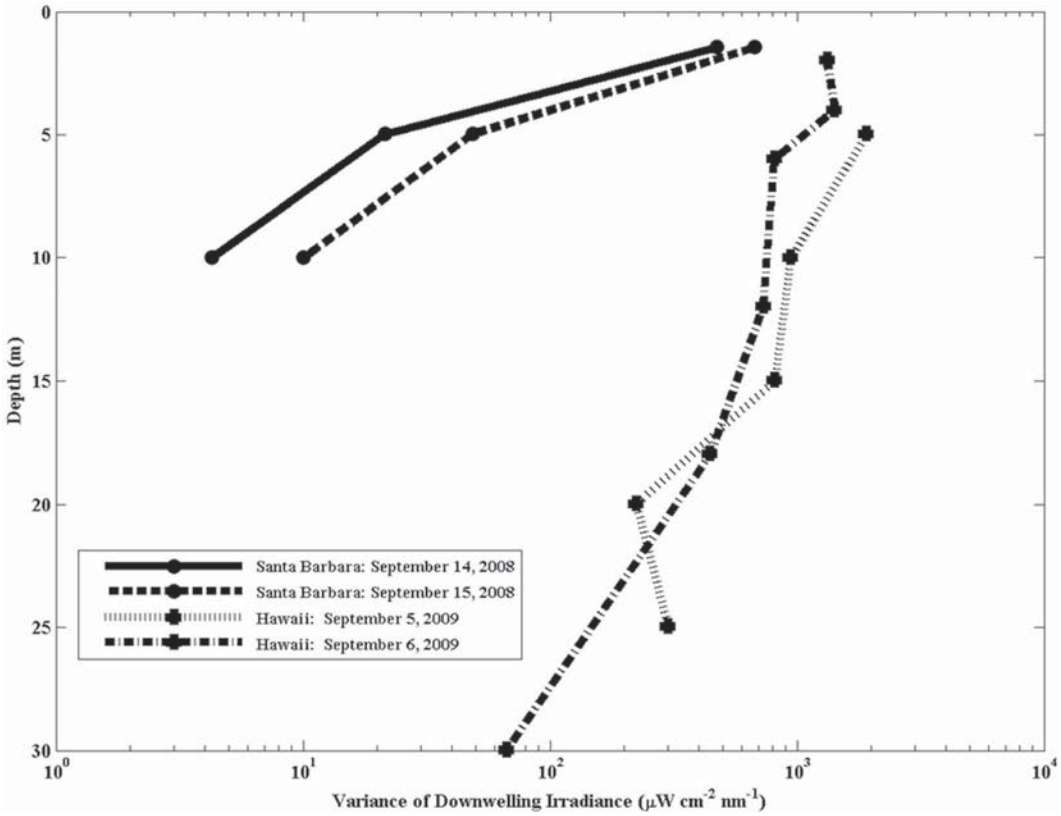

Figure 10. Variance in downwelling irradiance, $E_d(\lambda)$, measurements as a function of depth (m) made from the AUV for Santa Barbara Channel on 14 September and 15 September 2008 and off the Hawaiian Islands on 5 September and 6 September 2009.

amplitudes in $E_d(490)$ variance were depth dependent at the highest wave numbers. According to *Zaneveld et al.* [2001], the focal point of wave focusing can be approximated by the ratio of the wave amplitude to the wavelength. Given that the depth of influence was near the maximum operating depth of the AUV (80 m) with seas of 5 m, the maximum surface wavelength was on the order of 100 m. These results indicate that in fact the surface wavefield and wave focusing disproportionally influenced $E_d(490)$ across scales <1 m and at all depths, thus influencing the estimations of $K_d(490)$ and the derivations of $a_{ph}(\lambda)$ or $a_{cm}(\lambda)$. It should be noted that in Hawaii, had the vehicle been rated deeper than 100 m, that effective retrieval of $K_d(490)$ on these small scales for depths near the Chl *a* max depth (120 m) would have been likely.

4. Conclusion

[20] The use of AUVs to evaluate optical properties of the water column has been demonstrated by a number of investigators [see *Dickey et al.*, 2008]. These have included bio-optical proxy measures (i.e., Chl), measures of apparent optical properties [*Brown et al.*, 2004; *Wijesekera et al.*, 2005], and direct measures of IOPs [*Cunningham et al.*, 2003; *Wijesekera et al.*, 2005]. While these approaches have shown the value of AUVs in providing these measures with unprecedented resolution, it is important to evaluate the application of these techniques. The Santa Barbara Channel and waters off of Hawaii represented waters that are sequentially more optically transparent than the waters in the Mid-Atlantic Bight of *Brown et al.* [2004] and therefore provided reasonable locations for evaluation. In applying techniques by *Brown et al.* [2004], we found that this approach was marginally successful in the Santa Barbara Channel and not successful in deriving optical constituents in the near surface waters off of Hawaii. While the model approach remains valid, its application requires an assumption of a homogenous uniform light field for the retrieval of robust values for $K_d(\lambda)$ and subsequent inversion for deriving optical constituents. The $K_d(\lambda)$ values of *Brown et al.* [2004] were double those of this study for Santa Barbara Channel at 555 nm and fivefold larger at 412 nm. This along with uniform cloud cover and quiescent surface conditions provided ideal uniform light field condition to construct inversion approaches for the near surface. While this was an important exercise to move toward synoptic evaluation of the sub-surface spatial variability in optical constituents, the application has limited scope which is scaled with the combination of surface conditions and the water attenuation at a given locale. The optical conditions in the Santa Barbara Channel and off Hawaii demonstrated the influence of water attenuation, vehicle performance, variability in surface $E_d(\lambda)$ due to broken cloud cover, and wave focusing conditions on the ability to use inversion approaches of apparent optical properties over small scales to derive optical constituents in near surface waters. As the assumption of an uniform light field for deriving $K_d(\lambda)$ is not often met in both coastal and open ocean conditions, caution must be used in universally applying this method to other platforms such as Argo floats,

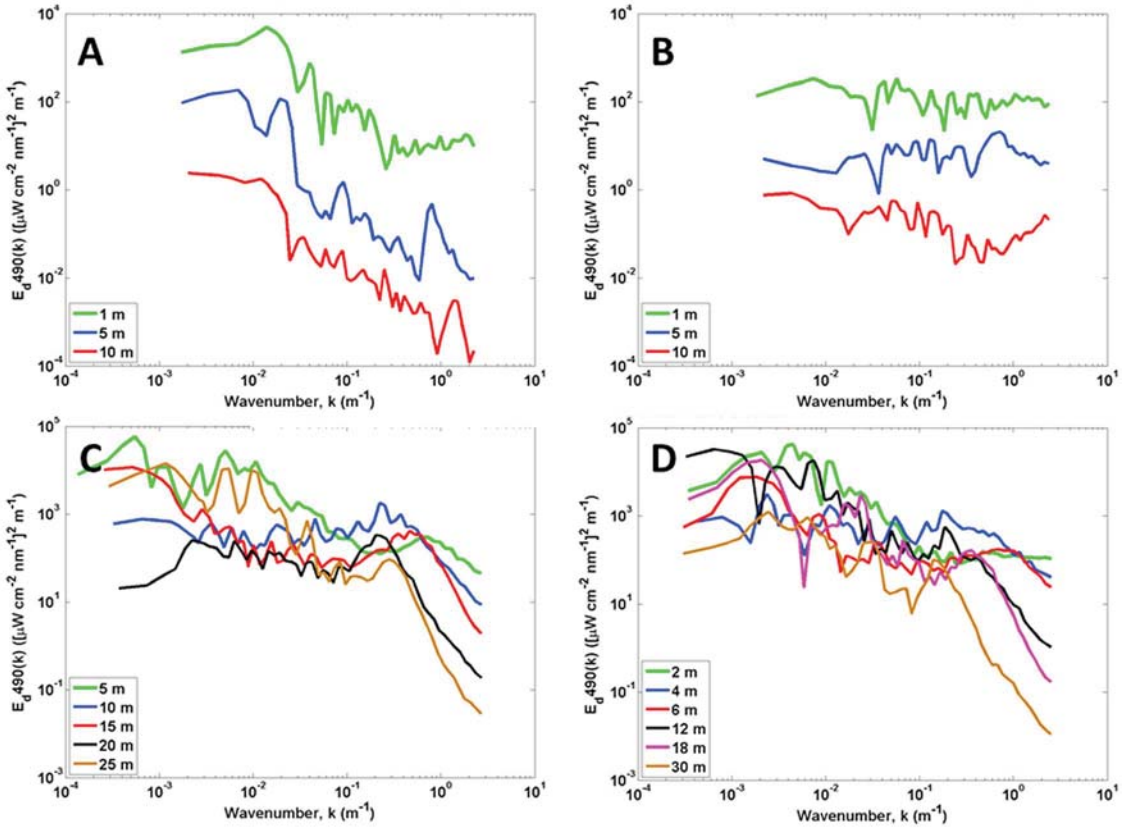

Figure 11. Horizontal wave number spectra of downwelling irradiance at 490 nm, $E_d(490)$, as a function of depth (m) following *Wijesekera et al.* [2005] for Santa Barbara Channel on (a) 14 September and (b) 15 September 2008 and off the Hawaiian Islands on (c) 5 September and (d) 6 September 2009.

profilers, gliders, and moorings as suggested by *Brown et al.* [2004]. It is important to note that while this study was focused on deriving optical constituents over small scales, the application of this method integrated over larger time and space scales on a variety of platforms may very well be applicable. As AUVs continue to develop and improve vehicle onboard power availability and duration, and sensors power requirements decrease, using AUVs to measure IOPs directly with active optics is an improved long-term strategy to address optical variability and biogeochemical processes over sub-mesoscales in the ocean.

[21] **Acknowledgments.** We thank the crew of the R/V *Kilo Moana* for their assistance in data collection. We also thank Jessica Connolly for assistance in the field effort in the Santa Barbara Channel and Johanna Weston for general assistance. This research was funded through the Office of Naval Research (ONR) project "Variability of near surface optical properties in high sea state conditions" under grant N00014-06-1-0070 to W. S. Pegau and M. Moline.

References

Leonard, N. E., D. A. Paley, F. Lekien, R. Sepulchre, D. M. Fratantoni, and R. E. Davis (2007), Collective motion, sensor networks, and ocean sampling, *Proc. IEEE*, *95*, 48–74, doi:10.1109/JPROC.2006.887295.

Blackwell, S. M., M. A. Moline, A. Schaffner, T. Garrison, and G. Chang (2008), Sub-kilometer length scales in coastal waters, *Cont. Shelf Res.*, *28*, 215–226, doi:10.1016/j.csr.2007.07.009.

Brown, A. C., H. Yannick, M. J. Purcel, J. J. Cullen, and M. R. Lewis (2004), Mapping coastal optical and biogeochemical variability using an autonomous underwater vehicle and a new bio-optical inversion algorithm, *Limnol. Oceanogr. Methods*, *2*, 262–281, doi:10.4319/lom.2004.2.262.

Ciotti, A. M., M. R. Lewis, and J. J. Cullen (2002), Assessment of the relationships between dominant cell size in natural phytoplankton communities and the spectral shape of the absorption coefficient, *Limnol. Oceanogr.*, *47*, 404–417, doi:10.4319/lo.2002.47.2.0404.

Coleman, T. F., and Y. Li (1994), On the convergence of interior-reflective Newton methods for nonlinear minimization subject to bounds, *Math. Program.*, *67*, 189–224, doi:10.1007/BF01582221.

Coleman, T. F., and Y. Li (1996), An interior trust region approach for nonlinear minimization subject to bounds, *SIAM J. Optim.*, *6*, 418–445, doi:10.1137/0806023.

Cudaback, C. N., and E. McPhee-Shaw (2009), Diurnal-period internal waves near Point Conception, California, *Estuarine Coastal Shelf Sci.*, *83*, 349–359, doi:10.1016/j.ecss.2008.12.018.

Cunningham, A., D. McKee, S. Craig, G. Tarran, and C. Widdicombe (2003), Fine-scale variability in phytoplankton community structure and inherent optical properties measured from an autonomous underwater vehicle, *J. Mar. Syst.*, *43*, 51–59, doi:10.1016/S0924-7963(03)00088-5.

Darecki, M., D. Stramski, and M. Sokólski (2011), Measurements of high-frequency light fluctuations induced by sea surface waves with an Underwater Porcupine Radiometer System, *J. Geophys. Res.*, *116*, C00H09, doi:10.1029/2011JC007338.

Dickey, T. D., et al. (1998), Initial results from the Bermuda Testbed Mooring program, *Deep Sea Res., Part I*, *45*, 771–794, doi:10.1016/S0967-0637(97)00096-4.

Dickey, T. D., E. C. Itsweire, M. A. Moline, and M. J. Perry (2008), Introduction to the *Limnology and Oceanography* special issue on autonomous and Lagrangian platforms and sensors (ALPS), *Limnol. Oceanogr.*, *53*, 2057–2061, doi:10.4319/lo.2008.53.5_part_2.2057.

Dong, C., Y. E. Idica, and J. C. McWilliams (2009), Circulation and multiple-scale variability in the Southern California Bight, *Prog. Oceanogr.*, *82*, 168–190, doi:10.1016/j.pocean.2009.07.005.

Gordon, H. R. (1989), Can the Lambert-Beer law be applied to the diffuse attenuation coefficient of ocean water?, *Limnol. Oceanogr.*, *34*, 1389–1409, doi:10.4319/lo.1989.34.8.1389.

Griffiths, G. (Ed.) (2002), *Technology and Applications of Autonomous Underwater Vehicles*, Taylor and Francis, New York, doi:10.1201/9780203522301.

Griffiths, G., R. Davis, C. Eriksen, D. Frye, P. Marchand, and T. Dickey (2001), Towards new platform technology for sustained observations, in *Observing the Oceans in the 21st Century*, edited by C. J. Koblinsky and N. R. Smith, pp. 324–338, GODAE, Bur. of Meteorol., Melbourne, Victoria, Australia.

Harding, L. W., B. B. Prézelin, B. M. Sweeney, and J. L. Cox (1982), Primary production as influenced by diel periodicity of phytoplankton photosynthesis, *Mar. Biol. Berlin*, *67*, 179–186, doi:10.1007/BF00401283.

Hibler, L. F., A. R. Maxwell, L. M. Miller, N. P. Kohn, D. L. Woodruff, M. J. Montes, J. H. Bowles, and M. A. Moline (2008), Improved fine scale transport model performance using AUV and HSI feedback in a tidally dominated system, *J. Geophys. Res.*, *113*, C08036, doi:10.1029/2008JC004739.

Kirkpatrick, G. J., C. Orrico, M. A. Moline, M. Oliver, and O. M. Schofield (2003), Continuous hyperspectral absorption measurements of colored dissolved organic material in aquatic systems, *Appl. Opt.*, *42*, 6564–6568, doi:10.1364/AO.42.006564.

Kostadinov, T. S., D. A. Siegel, S. Maritorena, and N. Guillocheau (2007), Ocean color observations and modeling for an optically complex site: Santa Barbara Channel, California, USA, *J. Geophys. Res.*, *112*, C07011, doi:10.1029/2006JC003526.

Krauss, T. P., L. Shure, and J. N. Little (1993), *Signal Processing Toolbox for Use With MATLAB*, MathWorks, Inc., Natick, Mass.

Maritorena, S., A. Morel, and B. Gentili (2000), Determination of the fluorescence quantum yield by oceanic phytoplankton in their natural habitat, *Appl. Opt.*, *39*, 6725–6737, doi:10.1364/AO.39.006725.

Marshall, B. R., and R. C. Smith (1990), Raman scattering and in-water ocean optical properties, *Appl. Opt.*, *29*, 71–84, doi:10.1364/AO.29.000071.

McGann, C., F. Py, K. Rajan, J. Ryan, H. Thomas, R. Henthorn, and R. McEwen (2009), Preliminary results for model-based adaptive control of an autonomous underwater vehicle, *Exp. Robotics*, *54*, 395–405, doi:10.1007/978-3-642-00196-3_46.

McManus, M. A., et al. (2003), Characteristics, distribution and persistence of thin layers over a 48 hour period, *Mar. Ecol. Prog. Ser.*, *261*, 1–19, doi:10.3354/meps261001.

Millie, D. F., O. M. Schofield, G. J. Kirkpatrick, G. Johnsen, P. A. Tester, and B. T. Vinyard (1997), Detection of harmful algal blooms using photopigments and absorption signatures: A case study for the Florida red tide dinoflagellate, Gymnodinium breve, *Limnol. Oceanogr.*, *42*, 1240–1251, doi:10.4319/lo.1997.42.5_part_2.1240.

Mitchell, B. G., M. Kahru, and J. Sherman (2000), Autonomous temperature-irradiance profiler resolves the spring bloom in the Sea of Japan, paper presented at Ocean Optics XV, Off. of Naval Res., Monte Carlo, Monaco, 16–20 Oct.

Moline, M. A., S. M. Blackwell, B. Allen, T. Austin, N. Forrester, R. Goldsborogh, M. Purcell, R. Stokey, and C. von Alt (2005), Remote Environmental Monitoring Units: An autonomous vehicle for characterizing coastal environments, *J. Atmos. Oceanic Technol.*, *22*, 1798–1809.

Moline, M. A., D. L. Woodruff, and N. R. Evans (2007), Optical delineation of benthic habitat using an autonomous underwater vehicle, *J. Field Robotics*, *24*, 461–471, doi:10.1002/rob.20176.

Moline, M. A., K. J. Benoit-Bird, I. C. Robbins, M. Schroth-Miller, C. M. Waluk, and B. Zelenke (2010), Integrated measurements of acoustical and optical thin layers: II. Horizontal length scales, *Cont. Shelf Res.*, *30*, 29–38, doi:10.1016/j.csr.2009.08.004.

Mueller, J. L., and G. S. Fargion (2002), Ocean optics protocols for satellite ocean color sensor validation, *NASA/TM-2002–688 21004/Rev3-Vol1*, rev. 3, part 1, p. 137, NASA Goddard Space Flight Cent., Greenbelt, Md.

Nencioli, F., G. Chang, M. Twardowski, and T. D. Dickey (2010), Optical characterization of an eddy-induced diatom bloom west of the island of Hawaii, *Biogeosciences 7*, 151–162, doi:10.5194/bg-7-151-2010.

Otero, M. P., and D. A. Siegel (2004), Spatial and temporal characteristics of sediment plumes and phytoplankton blooms in the Santa Barbara Channel, *Deep Sea Res., Part II*, *51*, 1129–1149.

Popa, D. O., A. C. Sanderson, R. J. Komerska, S. S. Mupparapu, D. R. Blidberg, and S. G. Chappel (2004), Adaptive sampling algorithms for multiple autonomous underwater vehicles, paper presented at IEEE Autonomous Underwater Vehicles Workshop, Inst. of Electr. and Electron. Eng., New York.

Pope, R. M., and E. S. Fry (1997), Absorption spectrum (380–700 nm) of pure water: II. Integrating cavity measurements, *Appl. Opt.*, *36*, 8710–8723, doi:10.1364/AO.36.008710.

Robbins, I. C., G. J. Kirkpatrick, S. M. Blackwell, J. Hillier, C. A. Knight, and M. A. Moline (2006), Improved monitoring of HABs using autonomous underwater vehicles (UUV), *Harmful Algae*, *6*, 931–943, doi:10.1016/j.hal.2006.03.005.

Roesler, C., and E. Boss (2003), Spectral beam attenuation coefficient retrieved from ocean color inversion, *Geophys. Res. Lett.*, *30*(9), 1468, doi:10.1029/2002GL016185.

Roesler, C., and M. J. Perry (1995), In situ phytoplankton absorption, fluorescence emission, and particulate backscattering spectra determined from reflectance, *J. Geophys. Res.*, *100*, 13,279–13,294, doi:10.1029/95JC00455.

Rudnick, D. L., and R. Ferrari (1999), Compensation of horizontal temperature and salinity gradients in the ocean mixed layer, *Science*, *283*, 526–529, doi:10.1126/science.283.5401.526.

Rudnick, D. L., and M. J. Perry (2003), ALPS: Autonomous and Lagrangian Platforms and Sensors, workshop report, p. 64, Geosci. Prof. Serv., Bethesda, Md. [Available at http://www.geo-prose.com/ALPS/report.html.]

Ryan, J. P., F. P. Chavez, and J. G. Bellingham (2005), Physical-biological coupling in Monterey Bay, California: Topographic influences on phytoplankton ecology, *Mar. Ecol. Prog. Ser.*, *287*, 23–32, doi:10.3354/meps287023.

Ryan, J. P., M. A. McManus, J. D. Paduan, and F. P. Chavez (2008), Phytoplankton thin layers caused by shear in frontal zones of a coastal upwelling system, *Mar. Ecol. Prog. Ser.*, *354*, 21–34, doi:10.3354/meps07222.

Sackmann, B. S., M. J. Perry, and C. C. Eriksen (2008), Seaglider observations of variability in daytime fluorescence quenching of chlorophyll-a in Northeastern Pacific coastal waters, *Biogeosci. Discuss.*, *5*, 2839–2865, doi:10.5194/bgd-5-2839-2008.

Sakamoto, C. M., D. M. Karl, H. W. Jannasch, R. R. Bidigare, R. M. Letelier, P. M. Walz, J. P. Ryan, P. S. Polito, and K. S. Johnson (2004), Influence of Rossby waves on nutrient dynamics and the plankton community structure in the North Pacific subtropical gyre, *J. Geophys. Res.*, *109*, C05032, doi:10.1029/2003JC001976.

Shcherbina, Y., M. C. Gregg, M. H. Alford, and R. R. Harcourt (2010), Three-dimensional structure and temporal evolution of submesoscale thermohaline intrusions in the North Pacific Subtropical Frontal Zone, *J. Phys. Oceanogr.*, *40*, 1669–1689, doi:10.1175/2010JPO4373.1.

Smith, K. S., and R. Ferrari (2009), The production and dissipation of compensated thermohaline variance by mesoscale stirring, *J. Phys. Oceanogr.*, *39*, 2477–2501, doi:10.1175/2009JPO4103.1.

Smith, R. C., K. J. Waters, and K. S. Baker (1991), Optical variability and pigment biomass in the Sargasso Sea as determined using deep sea optical mooring data, *J. Geophys. Res.*, *96*, 8665–8686.

Takahashi, M., and P. K. Bienfang (1983), Size structure of phytoplankton biomass and photosynthesis in subtropical Hawaiian waters, *Mar. Biol. Berlin*, *76*, 203–211, doi:10.1007/BF00392736.

Wijesekera, H. W., W. S. Pegau, and T. J. Boyd (2005), Effect of surface waves on the irradiance distribution in the upper ocean, *Opt. Express*, *13*, 9257–9264, doi:10.1364/OPEX.13.009257.

Yamashita, Y., and E. Tanoue (2009), Basin scale distribution of chromophoric dissolved organic matter in the Pacific Ocean, *Limnol. Oceanogr.*, *54*, 598–609, doi:10.4319/lo.2009.54.2.0598.

Yu, X., T. Dickey, J. Bellingham, D. Manov, and K. Streilein (2002), The application of autonomous underwater vehicles for interdisciplinary measurements in Massachusetts and Cape Cod Bays, *Cont. Shelf Res.*, *22*, 2225–2245, doi:10.1016/S0278-4343(02)00070-5.

Zaneveld, J. R. V., E. Boss, and A. Barnard (2001), Influence of surface waves on measured and modeled irradiance profiles, *Appl. Opt.*, *40*, 1442–1449, doi:10.1364/AO.40.001442.

M. A. Moline, I. Robbins, and B. Zelenke, Biological Sciences Department, California Polytechnic State University, 1 Grand Ave., San Luis Obispo, CA 93407, USA. (mmoline@calpoly.edu)

W. S. Pegau, Oil Spill Recovery Institute, PO Box 705, Cordova, AK 99574, USA.

H. Wijesekera, Naval Research Laboratory, Stennis Space Center, MI 39529, USA.